On the molecular basis of the activity of the antimalarial drug chloroquine: EXAFS-assisted DFT evidence of a direct Fe-N bond with free heme in solution

Giovanni Macetti,[a] Silvia Rizzato,[a] Fabio Beghi,[a] Lucia Silvestrini[b] and Leonardo Lo Presti[*a,c,d]*

[a] Università degli Studi di Milano, Department of Chemistry, Via Golgi 19, I-20133 Milano (Italy).

[b] University of Natural Resources and Life Sciences (BOKU), Wien, Department for Agrobiotechnology, Institute of Environmental Biotechnology and Department for Applied Genetics and Cell Biology, Konrad Lorenz Strasse 20, A-3430 Tulln/Donau (Austria).

[c] CNR-ISTM, Via Golgi 19, I-20133 Milano (Italy).

[d] Centre for Materials Crystallography, Århus University, Langelandsgade 140, DK-8000 Århus, (Denmark).

* To whom correspondence should be addressed. E-mail: leonardo.lopresti@unimi.it, Phone +39-02-50314252 Fax: +39-02-50314300.

Keywords: Antimalarial drugs, chloroquine, hematin, EXAFS, DFT calculations

ABSTRACT

4-aminoquinoline antiplasmodials interfere with the biocrystallization of the malaria pigment, a key step of the malaria parasite metabolism. It is commonly believed that these drugs set stacking π···π interactions with the Fe-protoporphyrin scaffold of the free heme, even though the details of the heme:drug recognition process remain elusive. In this work, the local coordination of Fe(III) ions in acidic solutions of hematin at room temperature was investigated by EXAFS spectroscopy in the 4.0-5.5 pH range, both in presence and in absence of the antimalarial drug chloroquine. EXAFS results were complemented by DFT simulations in polarizable continuum media (PCM) to model solvent effects. We found evidence that a complex where the drug quinoline nitrogen is coordinated with the iron center might coexist with formerly proposed adduct geometries, based on stacking interactions. Charge-assisted hydrogen bonds among lateral chains of the two molecules play a crucial role in stabilizing this complex, whose formation is favored by the presence of lipid micelles. The direct Fe-N bond could reversibly block the axial position in the Fe 1st coordination shell in free heme, acting as an inhibitor for the crystallization of the malaria pigment without permanently hampering the catalytic activity of the redox centre. These findings are discussed at the light of possible implications on the engineering of drugs able to thwart the adaptability of the malaria parasite against classical aminoquinoline-based therapies.

GRAPHICAL ABSTRACT. Difference between chloroquine-containing and chloroquine-free EXAFS spectra reveal the existence of a direct Fe–N coordinative bond with heme. DFT simulations show that this complex is stable in the acidic vacuolar environment and unstable in the alkaline cytosol, where uncomplexed heme increases the cellular oxidative stress of the malaria parasite.

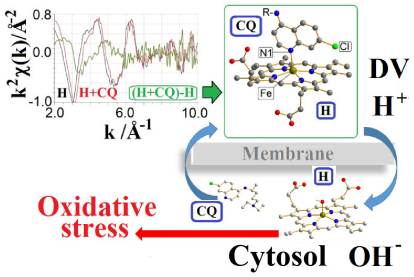

1. INTRODUCTION

Malaria, one of the topmost worldwide parasitic diseases, is caused by protozoa of the genus *Plasmodium*, which infect human erythrocytes via the transmission through the *Anopheles* mosquitoes and digest host hemoglobin. Despite ongoing efforts to counteract the contagion, the emerging and spreading of parasite (cross-)resistance [1] is becoming a dramatically serious problem. [2] In particular, *P. falciparum*, the most virulent malaria parasite, evolved resistance against chloroquine (CQ, Scheme I(a)), [3–5] an important aminoquinoline-class drug, [6] while other antiplasmodials are becoming less and less effective. [7–9] The urgency of designing new drugs able to thwart the parasite adaptability is growing up due to the need of limiting the infection. Additionally, in the next decades, the climate changes could provoke fresh outbreaks of the disease in Western countries and new malaria parasite adaptation processes cannot be excluded. [10]

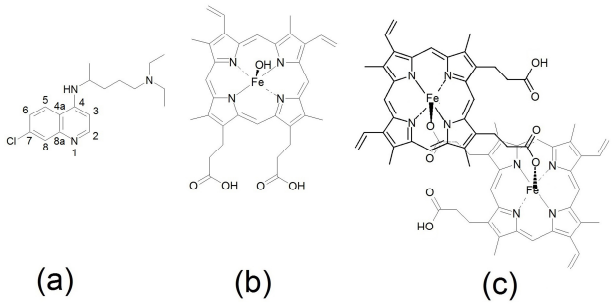

Scheme I. Chloroquine (a), hematin (b) and heme dimer (c) chemical structures

A possible weakness in the *Plasmodium* metabolic pathways resides in the fact that hemoglobin digestion releases free heme (Fe(II)-protoporphyrin IX, Fe(II)-PPIX). In the acidic (pH ≈ 4.5–5.0) digestive vacuole (DV) of the parasite, Fe-PPIX is present as monomeric hematin (Scheme I(b)), with partly dissociated propionic groups and oxidized Fe(III) active centres. This compound can be released into cytosol, where it takes part in cyclic Fenton-type redox reactions [11] generating reactive oxygen species (ROS) and increasing the cellular oxidative stress. [12,13] To detoxify free heme, the parasite promotes its dimerization through iron-carboxylate coordinative bonds

(Scheme I(c)) directly in the DV. [14,15] Dimeric heme then forms an insoluble solid known as β-hematin or hemozoin, which consists of triclinic ($P\bar{1}$) pale yellow crystals [16] that give a characteristic colour to the skin of malaria-infected people. It has been suggested that lipid nanodroplets dispersed in the DV might play a key role in the hemozoin self-assembly, [17,18] a process catalysed by a specific histidine-rich polymerase. [19,20]

Among other formerly proposed antiplasmodial mechanisms, [21,22] it is nowadays widely accepted that 4-aminoquinoline (AQ) drugs, such as CQ (Scheme I(a)), interfere with the parasite detoxification pathway. [23] A recent study of crystallization kinetics of β-hematin in presence of CQ argued [24] that the drug should act by binding at the fastest-growing crystal faces of hemozoin. Else, it is believed that CQ could hamper the heme dimerization in solution, even though there is no general consensus on the structure of the heme:CQ complex. [25–27] UV and UV-vis spectroscopy results on heme/CQ solutions are usually interpreted [28,29] by assuming that the rigid fused aromatic structure in the drug quinoline moiety interacts with the protoporphyrin scaffold through stacking π···π interactions. This structural model was corroborated by semiempirical AM1 [27] and PM3 [30] simulations. Also EXAFS [31,32] and NMR [25] experiments, although having been performed respectively on mesohematin anhydride solutions and in alkaline conditions, agree with this interaction geometry. On the contrary, high-grade DFT simulations suggest that either a water molecule or the OH^- group in hematin (Scheme I(b)) might act as a bridge between the iron centre and the secondary amine of CQ. [33] Direct Fe-N interactions were even proposed on the basis of solid state ^{13}C and ^{15}N NMR outcomes. [26] Attempts to produce crystalline heme:CQ adducts [24] were only partly successful, as up to now they led to the crystallization of a new β-hematin DMSO-solvated phase. On the contrary, adducts of Fe(III)-PPIX with other antimalarials (halofantrine,[34] quinine and quinidine [35]) have been successfully crystallized and their solid-state structures reported. Interestingly, in these structures Fe is always directly coordinated with a donor (O, N) atom of the drug. A very recent quantum

mechanical study of porphine and Fe-PPIX complexes accordingly predicted a direct Fe-N interaction when unsubstituted quinoline was considered as a ligand. [36]

Till now, no unequivocal evidence exists that secure the most probable heme:CQ interaction geometry. On the other hand, a complete understanding of this recognition process at the molecular and sub-molecular level is desirable to elucidate what kind of intermolecular interactions determine the antiplasmodial ability of CQ. To shed light on this issue, we report on a combined experimental and theoretical study of the hematin/CQ system in conditions as close as possible to the chemical environment of the Plasmodium DV. To elucidate the role of nanodispersed lipidic phases, samples including a tensioactive (sodium dodecyl sulphate, SDS) at its critical micellar concentration (CMC) were also compared with analogue tensioactive-free specimens. High-grade DFT simulation were crucial to interpret the very weak trends found by EXAFS experiments. This work represents the first *direct* and *systematic* investigation of the drug:substrate recognition process in the heme:CQ system, performed at a pH range comparable to the pH of the *Plasmodium* digestive vacuole. The most striking results of the present contribution are discussed in the perspective of engineering novel CQ-analogue drugs characterised by an improved specificity and effectiveness against malaria desease.

2. METHODS

2.1 Preparation of the solutions.

Solid powders of reagent-grade hematin porcine, CQ diphosphate salt and sodium dodecyl sulfate (SDS) were purchased by Sigma-Aldrich. The solutions were prepared by dissolving hematin in dimethylsulfoxyde (DMSO, reagent grade, Aldrich) and mixing 1:1 with an aqueous citrate buffer (final concentration: 0.1 M) to set the desired pH (4.0, 4.5, 5.0 and 5.5). The employment of a fully aqueous environment was not suitable, as hematin porcine was poorly soluble in water at the selected operative concentrations (see *infra*). For each pH value, three solutions were prepared,

consisting of hematin (H), hematin plus CQ (HC), and hematin plus CQ and SDS (HCS). Individual samples are labelled as X(pH), with X=H, HC or HCS. Where not otherwise specified, nominal concentration of hematin and CQ were set at 5 and 1 mM, respectively. More concentrated CQ solutions were also tested, but no significant differences were evident neither in the signal shape, nor in the fitting results (see Section S1 in the Supplementary Information, SI). The drug concentration is comparable with that reported *in vivo* within the DV of Plasmodium based on the estimated CQ vacuolar accumulation ratio. [27] In SDS-containing solutions, the critical micellar concentration of the tensioactive (8 mM) was set to have lipidic micelle coexisting with other reactants.

2.2 EXAFS experiments.

Extended X-ray Absorption Fine Structure (EXAFS) spectra across the Fe Kα absorption edge (7.11 keV) were carried out at the BM26A (DUBBLE) station of the ESRF facility in Grenoble (FR). All the spectra were recorded at room temperature in the 6.9-7.7 keV energy range, allowing a practical maximum resolution of 10.0 $Å^{-1}$ in k space. Glass capillaries (∅ 1.5 – 2.0 mm, ≈ 3/4 filled) were employed to host solutions. After some preliminary tests in transmission geometry, fluorescence mode was selected to maximize the signal intensity. See Section S1 SI for details concerning data collection (S1.1), and fitting (S1.2 – S1.5).

Great care was taken to avoid degradation of the solutions. All the specimens were either stored in the dark at T ≤ 4°C prior being sent to the experimental station, or measured as freshly prepared. To limit radiation damage (Section S1.1.2 SI), each recorded spectrum was obtained upon averaging a total of 6 scans, obtained from 2-3 repeated scans on a sequence of 2-3 capillaries filled with the same solution.

The Horae suite of programs, [37] based on the IFEFFIT library, [38] was used throughout data processing and fitting. The E_0 edge values were always set at the inflection point of the Fe $K\alpha$

transition. DFT-optimized structures of hematin, Fe(III)-protoporphyrin dimer and a sensible Fe(III)-protoporphyrin:CQ adduct (see Section 3.2 below and Section S1.3 SI) were employed as starting models to interpret the fine structure functions, whereas the available crystallographic data [16] were used to model the possible presence of hemozoin crystals. Hereinafter, we will refer to these structural models by Roman numerals as hematin monomer (i), heme dimer (ii), hemozoin (iii) and FePPIX:CQ adduct (iv). They were employed to perform both shell-by-shell and multi-shell fittings. Details on least-squares refinements can be found in Sections 4.2.1 and 4.2.2 below, whereas complete lists of statistical agreement factors and refined parameter values are available to the interested reader in Section S1.3 SI and Tables S1-S15 SI.

2.3 UV-Vis experiments.

The effect of CQ on the hematin-containing solutions was checked through UV-Vis spectroscopy. Measurements were performed by using a SPECTRO LGS53 UV-Vis spectrophotometer in the wavelength range of 300–450 nm. The concentrations of hematin and CQ drug were both 12 μM.

2.4 Quantum mechanical DFT simulations.

Quantum mechanical DFT calculations were performed by the Gaussian09 suite of programs [39] with the hybrid (U)B3LYP [40–43] functional and the triple-zeta 6–311G(p,d) basis set. [44] Calculations were performed in polarizable continuum media (PCM) [45] to take into account solvent effects at a reasonable computational cost. Geometry relaxations were performed both in water and in n-octanol as a model of an apolar environment. According with EPR and Mössbauer evidence, the iron centre was modelled in its oxidized form (Fe(III)) with spin multiplicity S = 5/2. [46,47] Main numerical results are summarized in Section S2 SI.

Fe(III)-protoporphyrin adducts with various chemical species, such as water, OH^- or chloroquine as axial ligands, were considered (see Section 4.3 below). To ensure that true minima on the

potential energy surface (PES) were reached, a full analysis of the normal vibration modes of each refined structure was carried out. Vibrational partition functions were also computed to provide thermochemical estimates [48] for ligand exchange and acid-base reactions on the iron centre.

3. RESULTS

Hereinafter, relevant chemical compounds are named by highlighting (i) the axial ligand in the iron first coordination shell, if present, and/or (ii) the protonation degree of the main acid/basic centres. For example, neutral hematin is indicated as $FePPIX(OH)H_2$, while $FEPPIX(OH)H^-$ and $FePPIX(OH)^{2-}$ mean that either or both the propionic groups have lost their protons. Similarly, $FePPIX(H_2O)H_2^+$ represents the protonated hematin molecule, with a water molecule coordinated on the Fe centre. In this notation, neutral chloroquine is written as CQ, while CQH^+ and CQH_2^{2+} are the corresponding single and double protonated forms.

3.1 UV-vis results

The recorded UV spectra (Figure 1) are identical to those reported in a same previous paper [49] carried out on 40% DMSO buffered aqueous solution of hematin and CQ in different stoichiometric ratios. In the presence of the drug we detected the same decrease of the Soret band of hematin at $\lambda \approx 400$ nm. According with Literature, [28,30,49**Errore. Il segnalibro non è definito.**] such an effect was attributed to the interference between the CQ drug and the heme monomer-dimer system, and in particular to the formation of some kind of donor-acceptor FePPIX-aminoquinoline supramolecular complex.

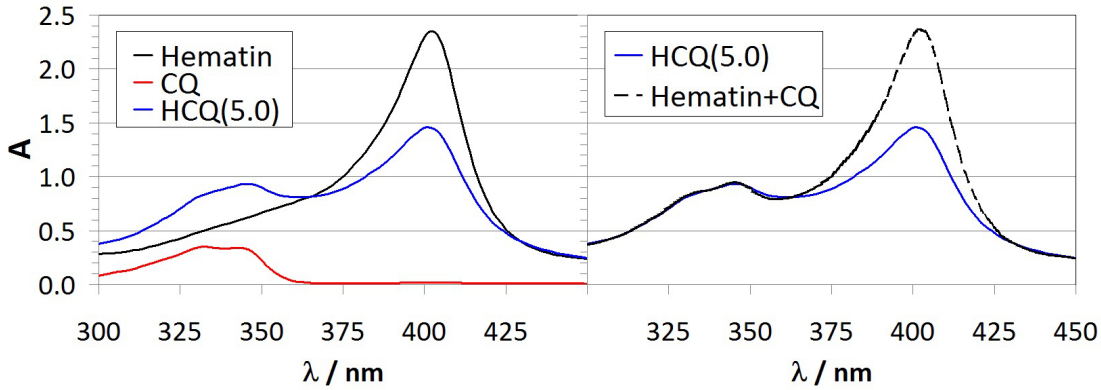

FIGURE 1. Colour online. Left: UV–vis spectra at pH = 5.0 of a 1:1 DMSO/aqueous citrate buffer solution (0.02 M) of CQ (red), hematin (black) and the binary mixture CQ/hematin (light blue). Right: Comparison of the spectrum of the binary mixture CQ/hematin (light blue) with the point-by-point sum signal computed from CQ and hematin spectra on the left (black, dashed).

3.2 EXAFS analysis.

Figure 2 shows the EXAFS fine structure functions, χ(k), and their corresponding Fourier transforms $\chi(R)$, for the pH = 5.0 series, taken as a representative case for the conditions of the DV environment. Analogous pictures for the other samples in the 4.0-5.5 pH range, including least-squares fits against the applied structural models, can be found in Section S1 SI (Figures S5-S12 SI), together with least-squares agreement factors (Tables S2-S4 SI) and final refined parameters (Tables S5–S15 SI).

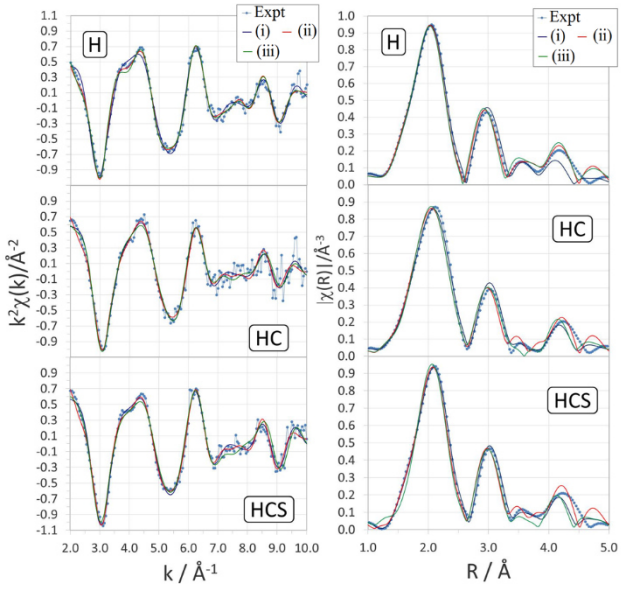

FIGURE 2. Colour online. k^2-scaled EXAFS fine structure functions $\chi(k)$ (left) and their Fourier transforms $\chi(R)$ (right) for the H(5.0), HC(5.0) and HCS(5.0) samples. Measured data are shown as blue dots, connected through broken lines as guides for the eye. The smoothed curves are functions employed to reproduce the experimental signals, as computed from the real-space fitting of different structural models against each dataset (blue: monomeric hematin, (i); red: heme dimer, (ii); green: crystalline hemozoin, (iii)).

At a first glance, the experimental $\chi(k)$ curves in Figure 2 look quite similar. The same holds true also for H, HC and HCS sample series at other pH's (Figures S5-S8 SI). Real-space Fourier transforms invariably show three main peaks at $R \approx 2.1$, 3.0 and 4.2 Å, plus minor oscillations hardly distinguishable from the Fourier noise due to k-space filtering. Accordingly, the experimental data might be fitted quite equally well by structural models based on monomeric hematin (i), dimeric heme (ii) and hemozoin crystals (iii). For example, the monomeric hematin model (i) gives R agreement factor / reduced χ^2 parameters as low as 0.017/32.6, 0.028/13.5 and 0.021/26.3 for the H(5.0), HC(5.0) and HCS(5.0) samples. To the sake of comparison, the same values become 0.016/28.0, 0.037/17.9 and 0.023/30.3 when computed on the basis of the dimeric heme model (ii). Crystalline hemozoin (iii) provides, on average, slightly worse statistics (Tables S2-S4 SI).

Neither obvious trends nor clear hints on what structural model(s) should be preferred to interpret the experimental data are easily recognizable (Tables S2-S4 SI). This is due to the fact that the local environment of the iron ion, which is fixed by the rigid protoporphyrin scaffold, necessarily dominates the EXAFS signals. Therefore, the main features of the iron coordination geometry must be conserved in all the examined samples. This implies that the recorded spectra are always similar to each other, and the effect of the drug should manifest in more subtle features throughout the dominating contributions of PPIX moiety. Besides, the picture is even more complicated by the fact that different iron complexes (monomeric hematin, dimeric heme, hemozoin and possible heme:CQ adducts) might coexist in solution. Nevertheless, some *systematic* trends are recognizable when the chemical composition of the solutions is varied.

Actually, most CQ-containing HC and HCS specimens have lower E_0 edge energies than the CQ-free ones (H) at a given pH (Table 1). Average $\langle E_0 \rangle$ values for the H, HC and HCS solutions throughout the 4.0-5.5 pH range turn out to be as high as 7125.6(5) eV, 7123.9(4) eV and 7124.3(3) eV respectively.

Table 1. E_0 edge values (eV) for the Fe $K\alpha$ transition in H, HC and HCS solutions as a function of pH.

pH	H[a]	HC[b]	HCS[c]
4.0	7126.5	7123.5	7125.0
4.5	7124.5	7123.0	7124.0
5.0	7126.5	7124.0	7124.5
5.5	7125.0	7125.0	7123.5

[a] Hematin-only solution
[b] Hematin plus chloroquine
[c] Hematin plus chloroquine and SDS

As each H, HC and HCS spectrum at a given pH is obtained from the average of 4-6 scans on 2-3 different solutions (see Section 2.2 above), it is improbable that this E_0 shift be due to random errors. Rather, though very small, in our opinion these differences likely rely on a true physical effect. Following other groups [31], we attributed them to a slight difference in the chemical environment of the iron absorber. The latter should be related to the presence of CQ in the reaction mixture. Accordingly, we did not apply any *a priori* shift to the EXAFS-estimated edge energies in the subsequent analysis.

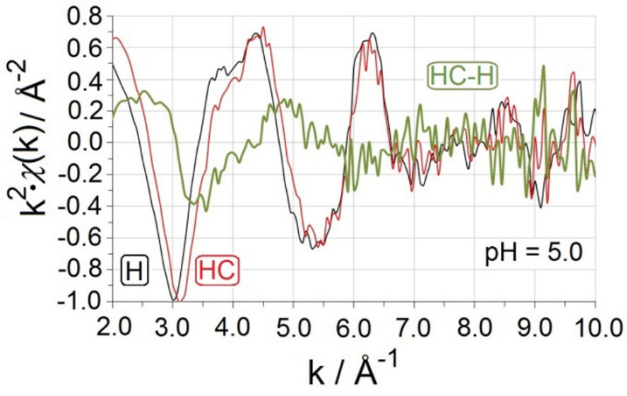

FIGURE 3. Colour online. Point-by-point difference (green) of the measured EXAFS fine structure functions of the HC(5.0) (red) and H(5.0) (black) specimens. See Figure S13-S16 SI for the corresponding curves at different pH's.

To single out statistically significant differences among the spectra recorded in the presence (HC, HCS) and in the absence (H) of chloroquine, the measured fine structure function of the CQ-free solution H might be subtracted from that of the CQ-containing one, *e.g.* HC, at the same pH. The residual signal should then convey the amount of information by which the two pristine spectra differ from each other, i.e. should enclose the effect of CQ on the environment of the iron ion. Figure 3 shows the point-by-point difference of the measured EXAFS fine structure functions of the HC and H solutions at pH = 5.0. An equivalent curve is obtained when the H(5.0) signal is subtracted from the HCS(5.0) one (Fig. S15(b) SI). In general, the difference signal shows neatly structured oscillations at low k values, due to the very small phase shift between the two original curves that can be traced back to the small differences in E_0 discusses above. On the contrary, at higher k modules these oscillations are smeared into featureless noise. It can be safely excluded that the difference signal in Fig. 3 could be attributed to other compounds in solution rather than CQ, such as DMSO or the citrate buffer, as both the HC and H samples contained exactly the same amount of these species within the statistical error. Moreover, identical findings hold true also when other samples are considered: A very similar difference signal is almost invariably retrieved throughout the whole 4.0-5.5 pH range, when either HC-H or the HCS-H differences are taken into account (Section S1.4 SI). However, difference spectra depend on the average structure of the solute throughout its accessible conformation spaces, which are likely different in H and HC (or HCS) samples. Besides, solvent effects and possible inhomogeneities of the probed specimens – all of them being potential sources of undetected but unavoidable systematic errors – might affect either the small detected phase shift or the intensity of the oscillations (Figures S13-S16 SI). For these reasons, extracting *quantitative* information from the difference signals is not feasible. Rather, on a more qualitative level, we note that two main peaks (A, C) at $R \approx 1.9$ and 2.8 Å, plus a neat shoulder (B) at ≈ 2.4 Å, appear in the real-space Fourier transform of the difference signal (Figure 4, left).

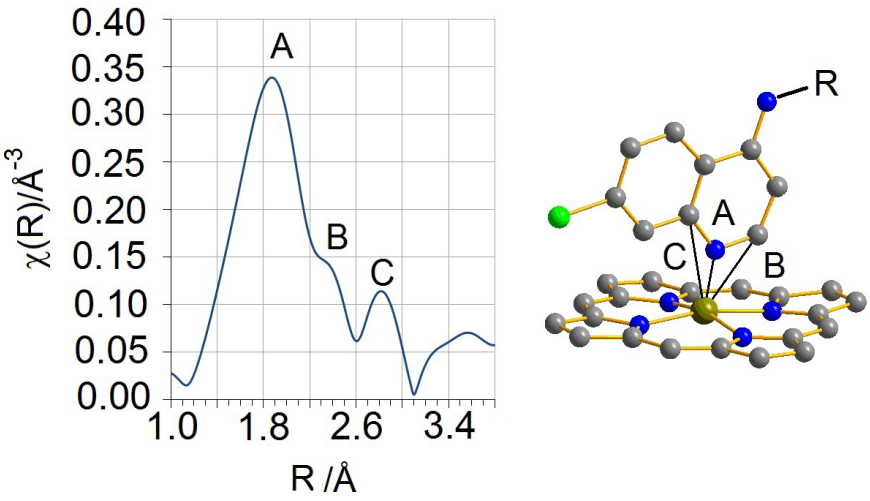

FIGURE 4. Colour online. Left: Real-space Fourier-transformed HC(5.0)-H(5.0) difference signal shown in Figure 3.. Right: Ball-and-stick representation (C: grey, N: blue, Cl: light green, Fe: brown) of the approximate (see text) interaction geometry for the quinoline ring of CQ and the FePPIX structure. –R stands for the CQ alkyl side chain. A, B and C label the features of the difference curve which correspond with the Fe–X (X = C, N) next neighbour distances on the right. Diamond v3.2k, © 1997-2014 Crystal Impact GbR, Bonn, Germany was employed throughout to draw ball-and-stick pictures.

Various models, based on possible approaching modes of the CQ molecule in the neighbourhood of the Fe(III) centre, were considered to interpret the main features in $\chi(R)$ (Figure 4, left). We eventually realized that such features, despite corresponding to *approximate* Fe-backscatterer distances, are *qualitatively* in accordance with the geometries of both the quinoline:porphine complex, as predicted by quantum mechanical calculations [36], and other PPIX:4-AQ drugs adducts, as determined by single-crystal X-ray diffraction experiments [34,35]. This prompted us to look for a FePPIX:CQ complex consistent with this interaction geometry, *i.e.* implying a direct Fe-N coordinative bond (Figure 4, right). Obviously, no quantitative insights into the heme:CQ recognition process can be obtained by the study of the difference signal alone. We therefore employed the information on the relative orientation between the quinoline and PPIX rings here hypothesized to build a suitable starting point for subsequent quantum mechanical DFT optimizations (see *infra*).

4. DISCUSSION: Is a Fe–N coordinative bond directly involved in the CQ:heme recognition process?

4.1 Quantum mechanical simulations.

To improve the accuracy of the proposed structural model (Figure 4, right), the adduct structure was optimized through DFT-PCM calculations of the isolated complex (see Section 2.4 above). Water and *n*-octanol were considered as solvents, the latter having being chosen to model the apolar environment due to lipid micelles in SDS-containing specimens. As for the starting geometry, we employed monoprotonated CQH^+ to bind the ferric centre through the free quinoline N atom. In general, the accessible conformation space for possible heme:CQ interacting pairs is very large, as the side hydrocarbon chain in CQH^+ has a significant torsional freedom even when N is coordinated to Fe. According to Literature findings, [25,33,50,51] to reduce the complexity of the problem to an affordable level we looked for favourable interaction geometries that included attractive N-H···O charge-assisted hydrogen bond (CAHB) interactions among the tertiary amine and the free heme propionate group.

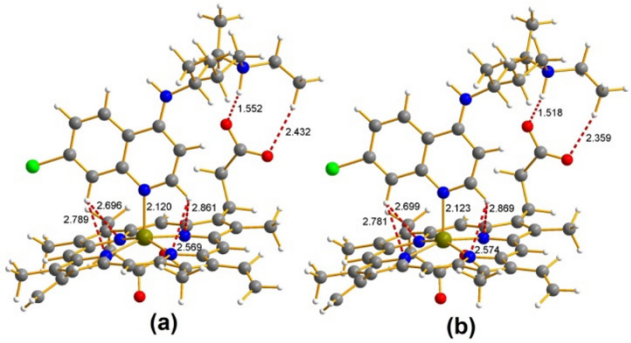

FIGURE 5. Colour online. Ball-and-stick representation of the B3LYP 6-311G(p,d) optimized geometry for a stable $FePPIX(CQH)H^+$ complex in water (a) and in n-octanol (b). Short NH···O, CH···O and CH···N intermolecular hydrogen-bonded contacts are shown as dashed red lines and the corresponding distances in Å highlighted. The usual colour code was employed to represent different atoms (green: chlorine, brown: iron; red: oxygen; blue: nitrogen; grey: carbon and white: hydrogen).

Figure 5 shows the fully relaxed geometries for the $FePPIX(CQH)H^+$ adduct corresponding to the true minima found by DFT simulations in water (a) and *n*-octanol (b) (Table S18 SI). The two complexes share the same basic structure, with the main molecular planes of PPIX and quinoline moieties lying approximately orthogonal to each other. The most striking difference is a significant reduction in the NH···O HB contact distances for the heme:CQ adduct in octanol (Fig.

5 and Tables S19-S20 SI). This effect is due to the expected increase in the CAHB strength in the low dielectric constant environment provided by the less polar solvent. On the contrary, the chemical nature of the solvent has clearly a minor effect on the Fe coordination environment, with changes in contact lengths between the FePPIX ring and the quinoline system not exceeding 10^{-2} Å.

4.2 Performance of the DFT structural models against EXAFS data.

4.2.1 First-shell fitting. To check to what extent the DFT-relaxed geometries shown in Fig. 5 reproduce the experimental data, we performed real-space fittings of the Fourier-transformed EXAFS fine structure functions (Tables 2–3, Figure 6). We focused just on the first peak at ≈ 2.0 Å (Figure 2, right), which is due to the convolution of structural contributions coming from the Fe(III) first-shell ligand sphere. On the basis of X-ray diffraction experiments on chloroquine-analogue complexes [34,35], solid state NMR findings [26] and our EXAFS-assisted DFT simulations (Sections 3.1 and 4.1 above), the first-sphere ligands are expected to be directly involved in the drug:substrate recognition process, while farther coordination shells should be much less affected by the presence of CQ. In-water DFT-optimized structures of (i) isolated hematin (FePPIX(OH)H^-), (ii) heme dimer (FePPIX(FePPIXH)H), (iii) crystalline hemozoin ([FePPIX(FePPIXH)H]$_{n\to\infty}$) and FePPIX(CQH)H^+ complex (iv) (Figure 5, left) were employed to compute starting estimates for the corresponding Fe–X (X = O, N) backscattering paths. As the Fe(III) ions in the PPIX scaffold exploit a C_{4v}-like distorted square-pyramidal coordination, two independent Δr corrections were applied to account for axial and equatorial ligands in models (i)–(iii). When the heme:CQ FePPIX(CQH)H^+ adduct model (iv) was considered, a third Δr parameter was added to simulate higher-R contributions due to the Fe-N_q backscattering path involving the quinoline N_q Nitrogen of CQ. Actually, this complex is expected to coexist in solution with drug-free substrates, such as monomeric hematin or dimeric heme.

Figure 6 and Table 2 show the structural parameters retrieved from the $\chi(R)$ signals fittings the hematin monomer (i) and heme:CQ adduct (iv) systems against H, HC and HCS sample series. Results corresponding to models (ii) and (iii) are very similar to those from model (i) and are reported in the Supporting Information (Figure S4 SI and Table S1 SI).

Table 2. Refined parameters for first-shell fittings against H, HC and HCS samples in the 4.0–5.5 pH range, with estimated standard deviations (e.s.d.'s) in parentheses. *R*- and *k*-windows were as large as 1.2-2.6 Å and 2-12 $Å^{-1}$, respectively. Hanning (dR = 0.0) and Kaiser-Bessel (dk = 1.89) filters were employed in the real and reciprocal spaces, giving a total of 16 independent points. Models (i) and (iv) were employed to interpret H and HC/HCS datasets, respectively. For the sake of comparison, the iron-ligand first-shell distances from DFT calculations in water are *d*[Fe–O] axial = 1.88 Å, <*d*[Fe-N]> equatorial = 2.071(3) Å, and *d*[Fe–N_q] axial = 2.12 Å.

Sample	*d*[Fe–O] axial / Å	<*d*[Fe-N]> equatorial/ Å	*d*[Fe–N_q] axial / Å [c]	S_0^2	σ /$Å^2$	R [d]
H(4.0) [a]	1.86(8)	2.03(2)	//	0.9(3)	0.006(6)	0.0715
HC(4.0) [b]	1.9(1)	2.02(2)	2.5(1)	1.1(6)	0.009(9)	0.0561
HCS(4.0) [b]	1.9(2)	2.01(5)	2.4(1)	1.6(8)	0.02(1)	0.0327
H(4.5) [a]	1.83(8)	2.02(2)	//	1.0(4)	0.007(6)	0.0634
HC(4.5) [b]	1.84(9)	2.03(2)	2.5(1)	1.2(9)	0.008(8)	0.0723
HCS(4.5) [b]	1.8(1)	2.04(2)	2.5(1)	1.2(9)	0.009(8)	0.0826
H(5.0) [a]	1.9(3)	2.00(5)	//	1.2(5)	0.02(2)	0.0409
HC(5.0) [b]	1.8(1)	2.03(2)	2.5(1)	1(1)	0.011(9)	0.0693
HCS(5.0) [b]	1.9(1)	2.05(2)	2.5(1)	1.2(8)	0.009(8)	0.0805
H(5.5) [a]	1.86(9)	2.04(2)	//	0.9(4)	0.005(6)	0.1090
HC(5.5) [b]	1.9(1)	2.04(3)	2.5(2)	1.2(8)	0.010(9)	0.0878
HCS(5.5) [b]	1.8(1)	2.02(3)	2.5(2)	1(1)	0.01(1)	0.0643

[a] Fitting against the hematin monomer $FePPIX(OH)H^-$ model (i) at the in-water optimized DFT geometry.
[b] Fitting against the The $FePPIX(CQH)H^+$ adduct model (iv) (Figure 5) at the in-water optimized DFT geometry.
[c] N_q is the quinoline Nitrogen of the CQ molecule.
[d] Statistical agreement factor.

The agreement among the refined structural parameters shown in Table 2 and the corresponding theoretical estimates is generally good. The Fe–N_q distances are clearly overestimated, even though their estimated standard deviations (e.s.d.'s) are so large that the theoretical expected values are retrieved within 2-3 e.s.d.'s in most cases.

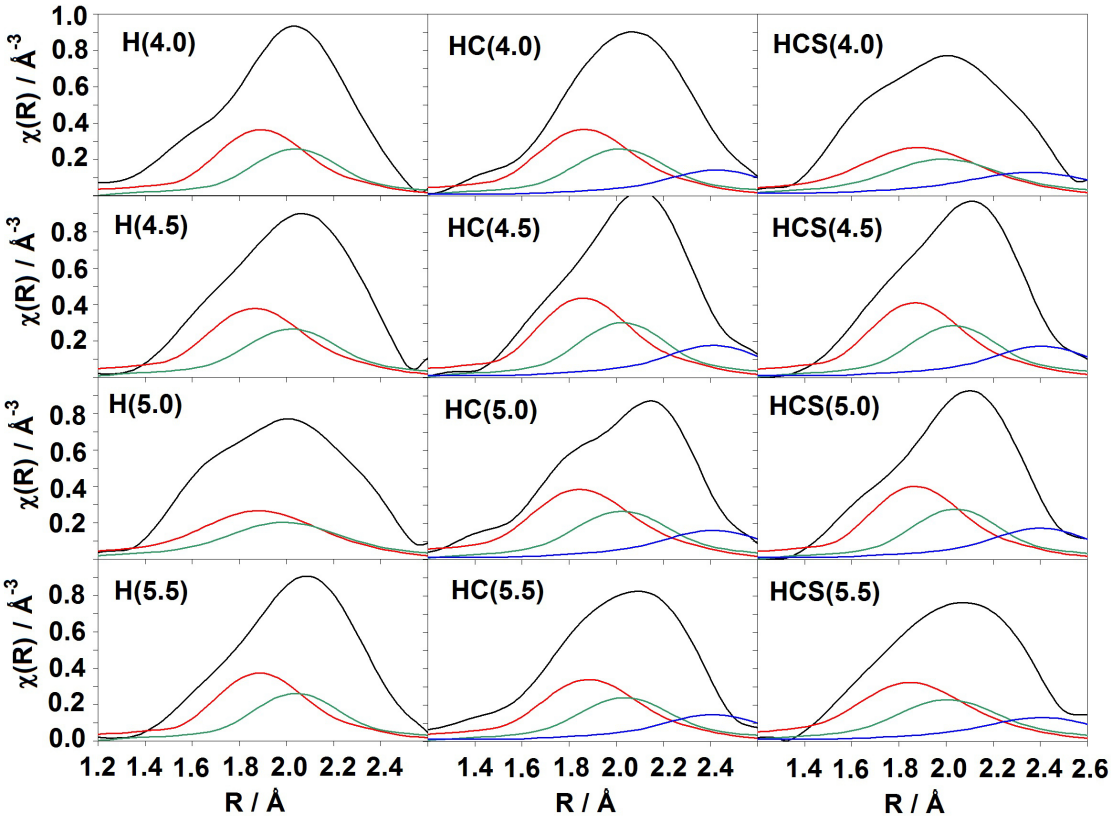

FIGURE 6. Colour online. $\chi(R)$ functions (black) for 1.2 Å ≤ R ≤ 2.6 Å, as computed from the EXAFS spectra of H, HC and HCS samples in the 4.0–5.5 pH range. The least-squares fitted contributions due to paths belonging to the Fe first coordination shell are also shown (red: Fe–O axial; green: <Fe–N> equatorial; light blue: Fe–N_q axial, N_q being the quinoline Nitrogen of CQ). The specs of the least-squares models are the same as in Table 2.

From Figure 6, it is evident that the square pyramidal first coordination shell of Fe in the PPIX scaffold dominates the $\chi(R)$ signal: Compare for example the individual path contributions for Fe–O axial (red) and Fe-N equatorial (green) scatterers in H samples with those in HC and HCS ones. As expected, the hypothesized N_q ligand provides just a minor correction to the $\chi(R)$ function. Accordingly, the corresponding contribution due to this path (light blue curves in Figure 6) is always very broad, and in fact its high variance translates into the high estimated standard deviations of the d[Fe–N_q] values in Table 2.

Yet, the following points are also worth of being noted. First, the maximum of the first-shell peak shows a slight tendency to be systematically shifted towards higher R backscattering lengths upon the addition of either CQ, or CQ and SDS. Second, the peak of HC and HCS samples is

systematically broader than in H solutions. The only exception is the pH = 5.0 series, whose H(5.0) parent solution shows an exceptionally broad first-shell peak compared with other H specimens. We note, however, that that even in this case the signals from HC(5.0) and HCS(5.0) solutions are neatly shifted towards higher *R* values with respect to H(5.0). These evidences might be traced back to the increasing importance of the high-*R* contribution of the Fe-N_q axial bond when the drug (and/or SDS) is present. It is improbable that such changes are due to π···π heme:CQ interactions, as the latter are expected to take place at considerably longer distances from the iron atom. For example, fittings against NMR data [25] give an estimate of 3.9(2) Å for the Fe–N_q distance in the heme:CQ adduct.

Unfortunately, the difference we observe can be hardly translated into a quantitative model, as the improvement of the fit quality against the HC and HCS data upon adding the Fe–N_q contribution is only marginal. Table 3 lists the individual agreement R factors, as computed after applying models (i)–(iv) to each chloroquine-containing HC and HCS dataset. Model (iv) invariably shows a slight improvement in the final R factor, as expected due to its higher number of variable parameters. To assess whether such an improvement is also statistically significant, the Hamilton R-test [52] was performed (Table 3, last column). Interestingly, the test is always satisfied, but the confidence level is generally low. It should be remarked that the EXAFS spectra here studied were recorded in dilute solution at room temperature.

Table 3. Agreement R factors when different structural models are applied to real-space EXAFS datasets H, HC and HCS. Global fitting parameters are the same as in Table 2 above. Models (i)–(iii) rely on 13 variables, which become 14 for the heme:CQ adduct one (iv) (see text). The number of independent points is always 16.

Model → Sample ↓	Hematin monomer (i)	Hematin dimer (ii)	Hemozoin (iii)	FePPIX(CQH)H^+ adduct (iv)	Average Hamilton significance level [a]
HC(4.0)	0.0705	0.0677	0.0692	0.0561	50.0 %
HCS(4.0)	0.0409	0.0441	0.0428	0.0327	66.7 %
HC(4.5)	0.0845	0.0801	0.0817	0.0723	50.0 %
HCS(4.5)	0.0987	0.0958	0.0968	0.0826	50.0 %
HC(5.0)	0.0959	0.0916	0.0940	0.0693	75.0 %
HCS(5.0)	0.0945	0.0927	0.0933	0.0805	50.0 %
HC(5.5)	0.1076	0.1070	0.1076	0.0878	50.0 %
HCS(5.5)	0.0792	0.0776	0.0790	0.0643	50.0 %

[a] Confidence level at which the Hamilton significance test [52] is satisfied, given as the average of the individual confidence levels for comparisons of model (iv) with models (i), (ii) and (iii), respectively. The higher this parameter, the higher the probability that the slight improvement of the agreement factor due to model (iv), which employs one more variable than models (i)–(iii), is statistically significant.

Therefore, thermal motion issues make very difficult to extract accurate and quantitative information from the least-squares fittings alone. On the other hand, we have weak, although *systematic*, indications that i) the presence of CQ (and of CQ plus SDS) somehow influence the first coordination shell of the iron absorber and ii) the proposed heme:CQ adduct model (iv) performs slightly better than (i)–(iii) in interpreting the measured signal.

4.2.2 Multi-shell fitting. It is instructive to explore the outcomes of multi-shell fittings as a function of the chemical composition of the probed solutions. This is indeed the method recently employed to interpret EXAFS spectra collected on mesohematin anhydride:CQ systems [31,32]. Moreover, due to above sketched difficulties in retrieving accurate geometric parameters at atomic resolution from experimental data, we might inspect at the performances exploited by each DFT model in reproducing a wider portion (1.0 Å ≤ R ≤ 5.0 Å) of the $\chi(R)$ function. In this way, a greater number of independent data can be taken into account, granting more flexibility to the model and allowing to retrieve at least qualitative hints on what species among the (i)–(iv) above described are favoured, on average, in a given chemical environment. Full details of the least-squares procedures, including individual statistics of the various fits, refined parameters (Tables S2–S15 SI) and first-shell coordination distances (Tables S21–S31 SI), can be found in Sections S1.3 and S3 SI.

To compare the quality of the various models on the same grounds, especially when applied to different samples, we define here for the first time a 'score function' for the i-th model, S_i, based on the reduced χ^2 parameters according to:

$$S_i = \frac{1}{n} \cdot \frac{\sum_{i=1}^{N} \chi_i^2 - \chi_i^2}{\sum_{i=1}^{N} \chi_i^2} \cdot 100 \qquad (1)$$

In (1), each sum runs over the N models applied to a given spectrum, n is an integer normalization constant to have $\Sigma_i S_i = 100$ and χ_i^2 is the reduced χ_i^2 of the i-th model. The lower an individual χ_i^2, the higher will be the corresponding score S_i, meaning that that model provides a better fit against the experimental fine structure function of a given sample than any other model with a lower score. Neither clear nor systematic trends are detectable among individual S_i (Figure S17 SI) estimates as a function of the pH. Therefore, just the average scores of each model throughout each pH series were considered. Figure 7 summarizes the computed scores for the models above listed against the H, HC and HCS sample series.

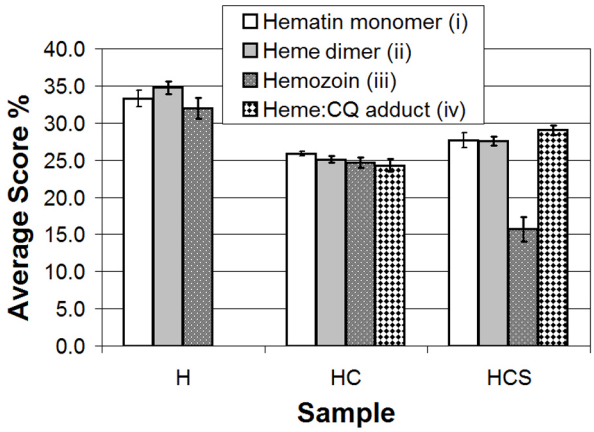

FIGURE 7. Color online. Suitability of different structural models in reproducing experimental EXAFS data for the H, HC and HCS sample series. Fitting ranges were always 1.0 Å ≤ R ≤ 5.0 Å and 2.0 Å $^{-1}$ ≤ k ≤ 10.0 Å $^{-1}$, corresponding to 25 independent data. Models (i)–(iii) employed 18 independent variables, which became 20 when model (iv) was considered.The higher the score parameter (eq. (1)), the better that model fits the specific sample that it is being considered (see text). Models (i)–(iv) described in Section 4.2.1 above were taken into account. Each bar comes from the average of individual score functions throughout the 4.0–5.5 pH range. Vertical lines correspond to 1 estimated standard deviation (e.s.d.).

Looking at trends of mean values in Figure 7 rather than at individual measurements (Figure S17 SI), some interesting indications can be retrieved. For example, when the drug is not present (H solution), models (i) and (ii) differ by ≈ 2 e.s.d.'s, with the heme dimer performing slightly better. This is no longer true when chloroquine is added to the mixture, as in HC solutions all the four models are, on average, equally performant. Comparing the HC series with the HCS out, on the contrary, it is evident that the presence of SDS significantly enhances the performances of the heme:CQ adduct

model, while the hemozoin model (iii) becomes absolutely the worst performing one. Incidentally, the fact that model (iii) invariably shows a poorer score with respect to (i) and (ii) (Figure 7) could be related to the absence of chemical promoters of the heme polymerization [19,20] in our model chemical mixture. The Hamilton R-test [52] is always satisfied when the model with more parameters (heme:CQ adduct) is compared with the roughly equally-performant models with less parameters, such as the hematin monomer (i) or dimer (ii) ones. The average significance level for all the samples indeed amounts to 80.5 ± 0.1% (comparison with model (i)) and increases up to 86.8 ± 0.1% upon comparison with model (ii). See Section S1.5 SI for more details.

In conclusion, the presence of lipidic micelle somewhat favours the formation of the heme:drug complex, discouraging at the same time the appearing of hemozoin crystals. This could be related to the increased strength of the CAHB non-covalent interactions among side chains (see above) in a low dielectric constant medium. According also with Literature findings, [53] the overall chemical composition of the DV environment (*e.g.* the presence of lipidic phases) appears to be more determinant than pH_{DV} alone for the molecular recognition process. It should be stressed that we do not demand the proposed model for the FePPIX(CQH)H^+ complex as the only possible. Former spectroscopic (EXAFS, NMR and UV-Vis) evidence implies that the setup of π···π stacking interactions between the quinoline moiety of CQ and the FePPIX aromatic system is indeed probable and it cannot be excluded that our proposed Fe–N interaction geometry coexist with stacked heme:CQ adducts in solution.

4.3 Suitability of the heme:drug complexation in the DV chemical environment.

To verify whether the formation of the proposed FePPIX(CQH)H^+ complex is possible in practice, it is important to take into account what reactions, and in particular which acid-base equilibria, are likely to occur in the *Plasmodium* vacuolar environment. pH_{DV} is expected to range from 4.5 to 5.5. [53–55] Under these conditions, the doubly protonated form of chloroquine,

CQH_2^{2+}, prevails over the monoprotonated (CQH^+) and neutral (CQ) forms (Section S4 SI, Figure S18 SI). [56,57] Indeed, the tertiary amine and quinoline basic centres in CQ (Scheme I(a)) have respectively $pK_a \approx 10.18$ and ≈ 8.38, [58] even though a lower pK_a (6.33) was also recently reported for the quinoline N atom. [54] Classical thermodynamic calculations show that the $[CQH^+]/[CQH_2^{2+}]$ ratio steeply increases by one order of magnitude (from $\approx 1 \cdot 10^{-4}$ to $\approx 1 \cdot 10^{-3}$) as the pH rises from 4.5 to 5.5 (Figure S19(a) SI), while the neutral CQ form is always at least two order of magnitude more diluted than CQH^+ (Figure S19(b) SI). Therefore, one may wonder whether enough monoprotonated drug, CQH^+, is present in the DV to effectively complex heme according to the geometry here proposed (see above).

To answer this question, it is worth noting that in the vacuolar environment free hematin ($FePPIX(OH)H^-$) undergoes a strongly exothermic protonation to give the corresponding neutral FePPIX-water complex ($FePPIX(H_2O)H$), which in turn might act as a reaction intermediate towards the heme:CQ adduct (reactions (2a-c)):

$$CQH_2^{2+} + H_2O \rightarrow CQH^+ + H_3O^+ \quad (2a)$$

$$FePPIX(OH)H^- + H_3O^+ \rightarrow FePPIX(H_2O)H + H_2O \quad (2b)$$

$$FePPIX(H_2O)H + CQH^+ \rightarrow FePPIX(CQH)H^+ + H_2O \quad (2c)$$

The latter sum to give the process (3):

$$FePPIX(OH)H^- + CQH_2^{2+} \rightarrow FePPIX(CQH)H^+ + H_2O \quad (3)$$

which is an acid-base reaction, coupled with a ligand exchange, between fully protonated chloroquine and free hematin. In other words, the monoprotonated minority form of drug, CQH^+, may form upon complexation with heme and it is not strictly required that it acts itself as a reactant.

Table 4. Thermochemical data (kJ·mol^{-1}) for reactions (2) and (3) at T = 298 K and p = 1 bar.[a]

Reaction	$\Delta_r H^{\varnothing}$	$\Delta_r G^{\varnothing}$	$T \cdot \Delta_r S^{\varnothing}$
(2a)	156.9	152.0	4.9
	155.1	148.7	6.5
(2b)	-139.2	-138.3	-0.9
	-169.5	-170.5	1.0
(2c)	-85.5	-49.2	-36.3
	-116.4	-80.0	-36.5
(3)	-67.8	-35.4	-32.4
	-130.8	-101.8	-29.0

[a] Thermochemical quantities are computed from the DFT electronic energies of reactants and products in water (first row) and n-octanol (second row) upon applying statistical thermodynamics corrections.

Table 4 shows the thermochemical data associated to reactions (2a-c) and (3), as computed at the DFT-B3LYP 6-311G(p,d) level of theory. Individual values of the quantum mechanical electronic energies are listed in the SI (Section S5, Tables S32–S34). Strictly speaking, entries in Table 4 refer to processes taking place among ideal gases of reagents and products [48] and therefore they cannot be directly compared with experimental outcomes. Yet, it is worth noting that our estimate for the reaction enthalpy of the overall reaction (3) among stable species in water (–16.2 kcal·mol^{-1}) is reasonably close to calorimetric measurements of heat associated to the heme:CQ binding process (–10(1) kcal·mol^{-1} at T = 37 °C and pH = 6.5 [59] and –7.9 kcal·mol^{-1} at T = 28 °C and pH = 5.6 [60]).

Data in Table 4 show that processes (2a-c) are all enthalpy-driven, and so the overall reaction (3), as the entropy term is either immaterial (2a-b), or even unfavourable (2c). The entropy reduction associated to the ligand shift reaction (2c) is clearly due to the loss of conformational freedom experienced by the drug upon complexation, as strong CAHB interactions between the tertiary amine and the propionate moiety (Fig. 5) lock otherwise free torsion angles of the long hydrocarbon chain. In conclusion, reaction (3) is exergonic as the strongly exothermic acid-base process (2b) and the ligand shift reaction (2c) provide enough energy to pay the highly unfavourable deprotonation cost of the CQH_2^{2+} species (reaction (2a)).

When the same thermochemical parameters are computed from reactants and products optimized in *n*-octanol (Table 4), analogue conclusions hold true but the process (3) becomes significantly more favoured. This is due to a couple of concomitant effects. First, the neutral heme:water intermediate, FePPIX(H_2O)H, is more stabilized (reaction (2b)) with respect to its charged reactants in the low-dielectric constant medium than in water (Table S34 SI); second, the ligand-shift reaction (2c) becomes more exothermic as the apolar environment allow the strengthening of CAHB interactions (Figure 5, Tables S19–S20 SI). This is also consistent with EXAFS results (Figure 7).

It should be also noted that the vacuolar pH range is ideal for promoting hemozoin crystallization. In fact, the two propionate groups of the FePPIX(OH)H_2 scaffold have pK_a = 4.3 and 5.5 [36]; free hematin is expected to exist mainly in either anionic FePPIX(OH)H^- or neutral FePPIX(H_2O)H form (reaction (2b)), where just the more acidic propionic function has lost its proton. Indeed, a single protonated carboxylic function per heme molecule (Scheme I(c)) is required to set up hydrogen-bonded chains in the hemozoin crystal. [16] Then, heme:CQ complexation is expected to be in competition with heme dimerization (4):

$$2\ \text{FePPIX}(H_2O)\text{H} \rightarrow \text{FePPIX}(\text{FePPIX})\text{H} + 2\ H_2O \qquad (4)$$

The latter is strongly exothermic and exergonic, with $\Delta H^{\varnothing}$ ($\Delta G^{\varnothing}$) = –44.9 (–46.6) kcal·mol^{-1} and –52.7 (–55.0) kcal·mol^{-1} in water and *n*-octanol (see Table S34 SI). Therefore, a robust thermodynamic driving force exists towards heme dimerization. This evidence complies well with the slight preference showed by H EXAFS data for the heme dimer model (ii) (see above). At the same time, it also implies that the competition of CQ for the Fe axial position should be *kinetic* in nature. This is reasonable, as a ligand exchange reaction (2c), possibly conjugated with a proton transfer (3), is expected to occur faster than a concerted ligand exchange involving two water molecules on two Fe centres (4). It is also worth noting that the parasite employs a specific polymerase to speed up hemozoin crystallization. [19,20] This implies that heme self-assembly is

by itself a relatively slower process compared with possible antagonist reactions, such as extrusion of free heme from DV and/or complexation with CQ.

4.4 On the reversibility of the direct Fe–N bond in the heme:CQ complex.

There is consensus on the fact that free hematin is detrimental to the malaria parasites. Monomeric Fe-PPIX indeed produces oxidant ROS in the cytosol [12,13] (see the Introduction above), and it was also found to inhibit the malarial form of the enzyme lactate dehydrogenase. [21] To preserve the activity of the Fe^{3+} redox centre, it is mandatory that the axial position of the Fe-PPIX complex be not blocked irreversibly by any ligand. Binding of Fe(III) by propionate groups, followed by irreversible hemozoin crystallization (see Introduction), is indeed the detoxification mechanism adopted by the malaria parasite. Therefore, reversible heme:drug complexation is mandatory to account for the CQ antiplasmodial ability.

It has been recently proposed that the heme:CQ complex is unstable in the parasite cytosol, where it might passively diffuse through the DV membrane following its natural concentration gradient. [61] The *Plasmodium* cytosol is weakly alkaline (pH ≈ 7.15(7)), [62] so in that environment the majority of free ($FePPIX(OH)^{2-}$) and complexed (FePPIX(CQH)) heme molecules bear charged propionic groups. At the same time, the concentration of the CQH^+ form of chloroquine is, on average, two order of magnitude higher than in the DV (Figure S18 SI). In these conditions, OH^- ions can effectively shift CQH^+ from the iron complex according to (5a–b):

$$FePPIX(CQH) + H_2O \rightarrow FePPIX(H_2O)^- + CQH^+ \quad (5a)$$

$$FePPIX(H_2O)^- + OH- \rightarrow FePPIX(OH)^{2-} + H_2O \quad (5b)$$

which sum to equation (6):

$$FePPIX(CQH) + OH^- \rightarrow FePPIX(OH)^{2-} + CQH^+ \quad (6)$$

Table 5 shows the corresponding thermochemical data for processes (5) and (6). As expected, here the entropic term is favourable for the shift reaction (5a), as the released free drug can span a

larger portion of its accessible conformation space. However, it is again an exothermic acid-base reaction, (5b), which provides the enthalpic driving force for making the overall process (6) exergonic.

Table 5. As Table 4 above for reactions (5) and (6) at T = 298 K and p = 1 bar.[a]

Reaction	$\Delta_rH^{\varnothing}$	$\Delta_rG^{\varnothing}$	$T{\cdot}\Delta_rS^{\varnothing}$
(5a)	99.6	71.2	28.5
(5b)	-265.4	-268.3	2.9
(6)	-165.7	-197.1	31.4

[a] Reactants and products were optimized in water.

In conclusion our thermochemical calculations, within the limits of the approximations here employed, demonstrate that the Fe–N direct interaction in the heme:CQ complex does not irreversibly block the Fe-PPIX redox centre, as the FePPIX(CQH) adduct is unstable with respect to exchange with OH^- ions in the slightly alkaline conditions of the cytosol.

CONCLUSIONS

We investigated the interaction of the antimalarial drug chloroquine (CQ) with heme in acidic 1:1 H_2O:DMSO solutions at room temperature by EXAFS spectroscopy. The chemical composition of the solutions was set in order to reproduce as closely as possible the conditions within the digestive vacuole (DV) of the malaria parasite. EXAFS outcomes were also complemented by DFT simulations in water and *n*-octanol to provide an interpretative framework of the spectroscopic data and to investigate the thermochemistry of heme:CQ complexation.

A broad consensus sustains the heme:CQ complexation as the core process of the drug activity against *Plasmodium* parasite. Heme:CQ adducts might indeed either cause *direct* damage to the parasite membranes, [22] or produce *indirect* damage by aiding toxic free heme [12,13] to be released into cytosol. As CQ interferes with hemozoin assembly, it makes more Fe-PPIX available to diffuse out of the DV either in its monomeric [12] or complexed [61] form. Heme:CQ

adducts are indeed expected to be unstable in the slight alkaline environment of the *Plasmodium* cytosol, [61] and our DFT calculations support this hypothesis.

As for the nature of the heme:CQ complex, phase shifts detected in the EXAFS signal between CQ-containing and CQ-free hematin solutions suggest that, at least in the conditions here adopted, the first coordination shell of the iron ion is closely involved in the drug:substrate recognition process. We propose that a complex where the quinoline nitrogen of the drug is coordinated to the iron center might coexist with other possible (*e.g.* $\pi\cdots\pi$ stacked) adduct geometries. It is the first time that a direct Fe-N bond, formerly hypothesized on the basis of solid-state NMR findings, [26] is observed in solution. However, the reader must be aware of the technical limits of the experiments we performed. First, EXAFS spectra were collected at room temperature; therefore, thermal motion issues limit both the accuracy and the precision of the refined parameters. Second, the changes we found in EXAFS spectra are very small and do not allow to extract quantitative information on the nature of the heme:CQ complex(es). Nevertheless, trends in edge energies, difference signals and $\chi(R)$ functions are consistent throughout the whole pH series here explored and agree with the heme:CQ adduct model here proposed on the basis of EXAFS-aided DFT calculations. Obviously, the latter could be either confirmed or falsified by further experimental evidences. Low-T EXAFS experiments are in order to gain further insights into the interaction of AQ-class drugs with heme and a forthcoming paper will be devoted to this topic.

In any case, DFT simulations demonstrate that charge-assisted hydrogen bonds (CAHBs) among the drug tertiary amine R_3NH^+ and the free propionate chain of the Fe-PPIX system are determinant in stabilizing the adduct. As expected, CAHBs are strengthened in a less polar environment. Therefore, the formation of the proposed heme:drug adduct should be favoured by the presence of lipid micelles. In conclusion, both the quinoline Nitrogen and the lateral chain of CQ are effective components of the drug pharmacophore and cooperate in determining its ability to hamper heme dimerization.

In computational works, the putative effectiveness of a CQ-like drug is often judged based on its heme-binding strength. [28] Anyhow, the ability of the drug to slow down heme self-recognition and self-assembly could be as much important as thermodynamics in determining the effectiveness of the antiplasmodial action. Therefore, provided that the CQ-induced toxicity is mainly due to free heme and not to interactions of the drug with other molecular targets, [21] it is not strictly mandatory that the heme:CQ adduct be the most stable on absolute grounds. Besides, with a regard to the inhibition kinetics determination, CAHBs might be even more crucial than direct interplay among the core moieties of the interacting molecules. These non-covalent interactions are ubiquitary in all the proposed heme:CQ interaction geometries [25,33,50,51]. In light of the described findings, it is plausible to consider the CAHBs strength engineering as an effective strategy towards the development of novel CQ-based antiplasmodials.

Acknowledgements

This work was partially funded by Chemistry Department at UNIMI by the Development Plan of Athenaeum grant – line B1 (UNIAGI 17777). The Italian supercomputing centre CINECA is to be acknowledged for having granted computing time through the ISCRA C program (project QUADRUG). Warm thanks are also due to the staff of the BM26A beamline at ESRF (Grenoble, FR) for the help provided during the acquisition of EXAFS spectra. Eventually, financial support from the Centre for Materials Crystallography (CMC) at Aarhus (DK) was very much appreciated.

REFERENCES

[1] White N J 2004 *J. Clin. Investig.* **113**, 1084

[2] Petersen I, Eastman R and Lanzer M 2011 *FEBS letters,* **585**, 1551

[3] Ecker A, Lehane A M, Clain J and Fidock D A 2012 *Trends Parasitol.* **28**, 504

[4] Tran C V and Saier M H Jr 2004 *Microbiology* **150**, 1

[5] Juge N, Moriyama S, Miyaji T, Kawakami M, Iwai H, Fukui T, Nelson N, Omote H and Moriyama Y 2015 *Proc. Nat. Acad. Sci.* **112**, 3356

[6] Farooq U and Mahajan R C 2004 *J. Vect. Borne Dis.* **41**, 45

[7] Ruengweerayut R, Phyo P, Uthaisin C, Poravuth Y, Binh T Q, Tinto H, Pénali L K, Valeca N, Tien N T, Abdulla S, Borghini-Furher I, Duparc S, Shin C-S and Flecknenstein L 2012 *New Engl. J. Med.* **366**, 1298

[8] Dondorp A M, Fairhurst R M, Slutsker L, MacArthur J R, Breman J G, Guerin P J, Wellems T E, Ringwald P, Newman R D and Plowe C V 2011 *New Engl. J. Med.* **365**, 1073

[9] Saleh G, Soave R, Lo Presti L and Destro R 2013 *Chem. Eur. J.* **19**, 3490

[10] Siraj A S, Santos-Vega M, Bouma M J, Yadeta D, Carrascal D R and Pascual M 2014 *Science* **343**, 1154

[11] Müller S 2004 *Mol. Microb.* **53**, 1291

[12] Koreny L, Obornik M and Lukes J 2013 *PLoS Pathog.* **9**, e1003088

[13] Kumar S and Bandyopadhyay U 2005 *Toxicol. Lett.* **157**, 175

[14] Egan T S, Corbrink J M, Egan J, Hearne G R, Marques H M, Ntenteni S, Sewell B T, Smith P S, Taylor D, Van Schalkwyk D A and Walden J C 2002 *Biochem. J.* **365**, 343

[15] Becker K, Tilley L, Vennerstorm J L, Roberts D, Rogerson S and Ginsburg H 2004 *Int. J. Parasitol.* **34**, 163

[16] Pagola S, Stephens P W, Bohle D S, Kosar A D and Madsen S K 2000 *Nature* **404**, 307

[17] Pisciotta J M, Coppens I, Tripathi A K, Sholl P F, Shiman J, Bajad S, Shulaev V and Sullivan D Jr 2007 *Biochem. J.* **402**, 197

[18] Ketchum M A, Olafson K N, Petrova E V, Rimer J D and Vekilov P G 2013 *J. Chem. Phys.*, **139**, 121911

[19] Lynn A, Chandra S, Malhotra P and Chauhan V S 1999 *FEBS Letters* **459**, 267

[20] Sullivan D J Jr, Gluzman I Y and Goldberg D E 1996 *Science* **271**, 219

[21] Read J A, Wilkinson K W, Tranter R, Sessions R B, and Brady R L 1999 *J. Biol. Chem.* **274**, 10213

[22] Sugioka Y, Suzuki M, Sugioka K and Nakano M 1987 *FEBS Letters* **223**, 251

[23] Slater A F G, Swiggard W J, Orton B R, Flitter W D, Goldberg D E, Cerami A and Henderson G B 1991 *Proc. Natl. Acad. Sci. USA* **88**, 325

[24] Gildenhuys J, Roex T, Egan T J and De Villiers K A 2013 *J. Am. Chem. Soc.* **135**, 1037

[25] Leed A, DuBay K, Ursos L M B, Sears D, de Dios A C, and Roepe P D 2002 *Biochemistry* **41**, 10245

[26] De Dios A C, Tycko R, Ursos L M B and Roepe P D 2003 *J. Phys. Chem. A* **107**, 5821

[27] Warhurst D C, Craig J C, Adagu I S, Guy R K, Madrid P B and Fivelman Q L 2007 *Biochem. Pharmacol.* **73**, 1910

[28] Egan T J 2006 *J. Inorg. Biochem.* **100**, 916

[29] Frosch T, Schmitt M, Bringmann G, Kiefer W and Popp J 2007 *J. Phys. Chem. B* **111**, 1815

[30] Otelo V A, Sant'Ana A C, de Faria D L A and Menezes C M S 2011 *Bioorg. Med. Chem. Lett.* **21**, 250

[31] Walczak M S, Lawniczak-Jablonska K, Wolska A, Sienkiewicz A, Suarez L, Kosar A J and Bohle D S 2011 *J. Phys. Chem. B* **115**, 1145

[32] Walczak M S, Lawniczak-Jablonska K, Wolska A, Sikora M, Sienkiewicz A, Suárez L, Kosar A J, Bellemare M–J, Bohle D S 2011 *J. Phys. Chem. B* **115**, 4419

[33] Acharige A M D S D and Durrant M C 2014 *Transition Met. Chem. Dordrecht, Netherlands* **39**, 721

[34] de Villiers K A, Marques H M and Egan T J 2008 *J. of Inorg. Biochem.* **102**, 1660

[35] de Villiers K A, Gildenhuys J and le Roex T 2012 *ACS Chem. Biol.* **7**, 666

[36] Durrant M C 2014 *Dalton Trans.* **43**, 9754

[37] Ravel B and Newville M 2005 *J. Synchrotron Radiat.* **12**, 537

[38] Newville M 2001 *J. Synchrotron Radiat.* **8**, 322

[39] Frisch M J, Trucks G W, Schlegel H B, Scuseria G E, Robb M A, Cheeseman J R, Scalmani G, Barone V *et al*. 20009 Gaussian 09, Revision D.01, Gaussian, Inc., Wallingford CT

[40] Becke A D 1993 *J. Chem. Phys.* **98**, 5648

[41] Lee C, Yang W and Parr R G 1988 *Phys. Rev. B* **37**, 785

[42] Vosko S H, Wilk L and Nusair M 1980 *Can. J. Phys.* **58**, 1200

[43] Stephens P J, Devlin F J, Chabalowski C F and Frisch M J 1994 *J. Phys. Chem.* **98**, 11623

[44] Krishnan R, Binkley J S, Seeger R and Pople J A1980 *J. Chem. Phys.* **72**, 650

[45] Tomasi J, Mennucci B and Cammi R 2005 *Chem. Rev.* **105**, 2999

[46] Sienkiewicz A, Krzystek J, Vileno B, Chatain G, Kosar A J, Bohle D S and Forro L 2006 *J. Am. Chem. Soc.* **128**, 4534

[47] Bohle D S, Debrunner P, Jordan P A, Madsenand S K and Schulz C E 1998 *J. Am. Chem. Soc.* **120**, 8255

[48] Ochterski J W 2000 *Thermochemistry in Gaussian*, Gaussian Inc. pp. 1–19.

[49] Dascombe M J, Drew M G B, Morris H, Wilairat P, Auparakkitanon S, Moule W A, Alizadeh-Shekalgourabi S, Evans P G, Lloyd M, Dyas A M, Carr P and Ismail F M D 2005 *J. Med. Chem.* **48**, 5423

[50] Asghari-Khiavi M, Vongsvivut J, Perepichka I, Mechler A, Wood B R, McNaughton D and Bohle D S 2011 *J. Inorg. Biochem.* **105**, 1662

[51] Portela C, Afonso C M M, Pinto M M M and Ramos M J 2003 *FEBS Lett.* **547**, 217

[52] Hamilton W C 1965 *Acta Crystallogr.* **18**, 502

[53] Hayward R, Saliba K J and Kirk K 2006 *J. Cell Sci.* **119**, 1016

[54] Rendal C, Kusk K O and Trapp S 2011 *Environ. Toxicol. Chem.* **30**, 354

[55] Becker K, Tilley L, Vennerstrom J L, Roberts D, Rogerson S and Ginsburg H 2004 *Int. J. Parasitol.* **34**, 163

[56] Accordingly, it has been suggested that drug DV accumulation is due to the lower ability of the doubly protonated charged form in crossing the vacuolar membrane. See ref. 57.

[57] Hoang A N, Sandlin R D, Omar A, Egan T J and Wright D W 2010 *Biochemistry* **49**, 10107

[58] Warhurst D C, Steele J C P, Adagu I S, Craig J C and Cullander C 2003 *J. Antimicrob. Chemother.* **52**, 188

[59] Dorn A, Vippagunta S R, Matile H, Jaquet C, Vennerstrom J L and Ridley R G 1998 *Biochem. Pharmacol.* **55**, 727

[60] Vippagunta S R, Dorn A, Matile H, Bhattacharjee A K, Karle J M, Ellis W Y, Ridley R G and Vennerstrom J L 1999 *J. Med. Chem.* **42**, 4630

[61] Haynes R K, Cheu K-W, Chan H -W, Wong H-N, Li K-Y, Tang M M-K, Chen M-J, Guo Z-F, Guo Z-H, Sinniah K, Witte A B, Coghi P and Monti D 2012 *ChemMedChem* **7**, 2204

[62] Kuhn Y, Rohrbach P and Lanzer M 2007 *Cell. Microbiol.* **9**, 1004